Materials Advances

ROYAL SOCIETY OF CHEMISTRY

PAPER

Published on 17 August 2026

Cite this: DOI: 10.1039/d6ma01168c

Selective production of CO_2-free hydrogen gas and formate from ethylene glycol over supported Ru catalysts

Shivam Mishra, [a] Tushar A. Kharde, [a] Ankit Kumar, [ab] Uday Deshpande [c] and Sanjay K. Singh *[a]

Received 4th August 2026,
Accepted 13th August 2026

DOI: 10.1039/d6ma01168c

rsc.li/materials-advances

Developing energy-efficient, carbon-neutral routes to hydrogen production is critical for industrial deployment. Here, we demonstrate selective reforming of aqueous ethylene glycol (EG) to produce CO_2-free hydrogen and formate over ruthenium nanoparticles supported on $La(OH)_3$. Under alkaline conditions, $Ru/La(OH)_3$ delivers 2.94 mol H_2 per mol EG and ~94% yield of sodium formate (SF) at 130 °C. Under bulk reaction conditions, the catalyst achieves a hydrogen productivity of 350 $L(H_2)$ $g(Ru)^{-1}$ and a hydrogen production rate of 2359 $mmol(H_2)$ $g(Ru)^{-1}$ h^{-1} (~58 $L(H_2)$ $g(Ru)^{-1}$ h^{-1}) at this mild temperature. The process was also utilized for the depolymerization of polyethylene terephthalate (PET) waste, enabling CO_2-free hydrogen production alongside formate and terephthalate. Overall, these results highlight $Ru/La(OH)_3$ as a promising catalyst for sustainable hydrogen production from EG-based feedstocks.

1. Introduction

Rising energy demand, accelerating climate change, and the depletion of non-renewable resources have intensified the search for sustainable energy solutions.[1–3] Hydrogen (H_2) is an attractive clean energy carrier; however, it is rarely available in its free form and is typically bound in compounds, making its production energy-intensive and often associated with greenhouse-gas emissions.[4,5] Accordingly, renewable, biomass-derived feedstocks such as alcohols and polyols are being explored as sustainable and cost-effective sources of H_2.[6] Considerable attention has been devoted to C_1 liquids (*e.g.*, formic acid,[7–10] formaldehyde,[11–13] and methanol[14–17]) for on-demand H_2 production, storage, and transport because they are inexpensive, widely available, and liquid under ambient conditions.[18] In parallel, polyols such as ethylene glycol (EG), glycerol, sorbitol, and xylitol have emerged as renewable, easily handled H_2 sources due to their high hydrogen content. Among them, EG is particularly appealing because of its high H/C ratio, complete miscibility with water, and chemical stability under mild conditions, which make it a strong candidate for aqueous-phase reforming (APR).[19,20] In addition, EG can be selectively upgraded to value-added chemicals (*e.g.*, oxalic acid, glycolic acid, and formic acid), enabling integrated H_2 production with co-production of high-value chemicals.[21]

A wide range of catalysts have been investigated for H_2 production from EG, with major efforts aimed at suppressing undesired by-products such as CO, CO_2, and CH_4. Homogeneous systems based on Ru,[22–24] Ir,[25] and Mn[26] have also been explored for EG to H_2 transformation; for example, Ru-NNN pincer and N-heterocyclic carbene (NHC)-based complexes operate efficiently under alkaline conditions. However, homogeneous catalysis is often limited by catalyst recovery, potential product contamination, and incomplete selectivity, frequently giving glycolic acid (GA) as the major product.[22] These limitations have motivated the development of heterogeneous catalysts, which offer improved recyclability and stability and can deliver comparatively purer H_2. Numerous supported catalysts (*e.g.*, Ru/Al_2O_3,[27] $Pt–Ni/Al_2O_3$,[28] $Ni/CeO_2–Al_2O_3$,[29] Pt/Al_2O_3,[30] and related systems[31–34]) have been explored, although many of them require high reaction temperatures (>250 °C). APR provides a milder approach and has been demonstrated with catalysts such as Cu/CNF,[18] Ni/CNF,[18] Co/ZnO,[35] $Pt–Co/CeO_2–ZrO_2$,[36] Pt–Mn/CMK-3,[37] M/SiO_2 (M = Ni, Pt, Pd, Ru, Rh),[38] and RANEY®-NiSn.[39] Nonetheless, side reactions can still generate CO, CO_2 and light alkanes, lowering the H_2 yield and purity. Complementary studies have shown that EG can be converted to valuable C_1/C_2 products *via* selective C–C bond cleavage (Scheme 1a).[22] For example, Pt/Al_2O_3 enables EG reforming (225 °C, 90% conversion, 96% selectivity), but produces CO,

[a] *Catalysis Group, Department of Chemistry, Indian Institute of Technology Indore, Khandwa Road, Simrol, Indore, 453552, M.P., India. E-mail: sksingh@iiti.ac.in*
[b] *Institute for Inorganic Chemistry, Karlsruhe Institute of Technology, Engesserstr. 15, 76131, Karlsruhe, Germany*
[c] *UGC-DAE Consortium for Scientific Research, Indore, 452001, MP, India*

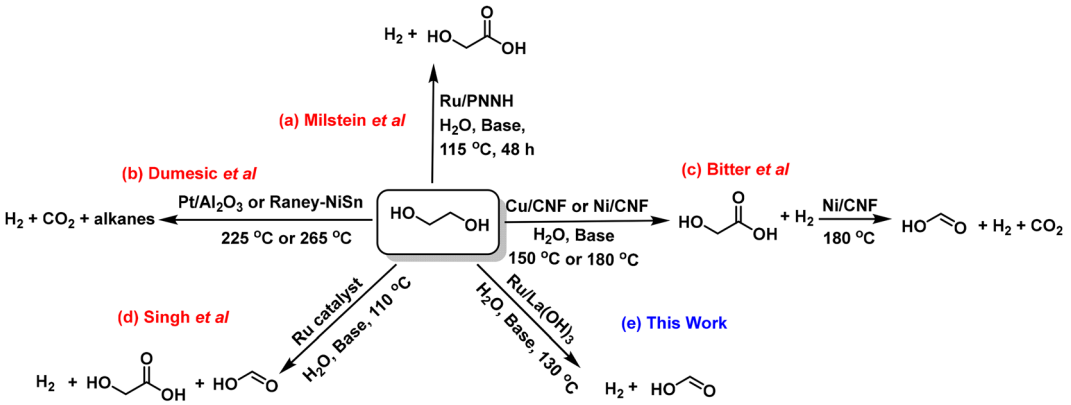

Scheme 1 Catalytic hydrogen production from ethylene glycol.

CO_2, and CH_4 (Scheme 1b).[30] Bitter *et al.* addressed this by a two-step route—EG to GA over Cu/CNF, followed by glycolic acid (GA) to formic acid (FA) and H_2 over Ni/CNF—with up to 99% H_2 selectivity (Scheme 1c).[18] Building on these advances, we recently reported a low-temperature heterogeneous Ru-based system operating at 110 °C; however, GA remained a minor side product (Scheme 1d).[40]

To address these challenges and further enhance H_2 yield from EG at low temperature, we developed a catalyst comprising ruthenium nanoparticles dispersed on $La(OH)_3$. The Ru/$La(OH)_3$ catalyst selectively converts EG to CO_2-free H_2 and formate at <140 °C, markedly lower than conventional EG reforming processes (>200 °C). We propose that surface hydroxyl groups on $La(OH)_3$ promote favorable interactions with EG and key intermediates, while Ru provides the dehydrogenation sites, together enabling selective low-temperature reforming. The catalyst delivered high turnover numbers and productivity under both recycling and bulk reaction conditions. Finally, we also utilized this process to demonstrate H_2 production from EG-based feedstock (PET waste) under analogous conditions.

2. Experimental section

2.1. Materials

$RuCl_3{\cdot}3H_2O$ ($>99\%$), $NaBH_4$ (98%), $La(OH)_3$ (99.9%), TiO_2 (99.5%), ZrO_2 (99%), and ethylene glycol ($>99\%$) were purchased from Sigma-Aldrich (India). High-purity argon was obtained from Sigma Gases (India). All other reagents and metal salts were commercially available and used as received without further purification.

2.2. Catalyst synthesis

Supported Ru catalysts were prepared by wet impregnation followed by a chemical reduction method, using $La(OH)_3$, γ-Al_2O_3, ZrO_2, CeO_2, and TiO_2 as supports. Typically, 90 mg of support was dispersed in 5 mL of distilled water in a 25 mL round-bottom flask and sonicated for 20 min. $RuCl_3{\cdot}6H_2O$ (0.1 mmol) was then added, and the mixture was stirred at room temperature for 12 h. An aqueous $NaBH_4$ solution (0.040 g in 5 mL water) was added dropwise under sonication to reduce Ru(III) to Ru(0). The resulting suspension was sonicated for an additional 30 min, after which the catalyst was collected by centrifugation, washed thoroughly with distilled water, and dried under vacuum prior to catalytic testing. The Ru loading was quantified by ICP-OES (average of three independent measurements; Table S2).

2.3. Catalyst characterization

Transmission electron microscopy (TEM) and energy-dispersive X-ray spectroscopy (EDS) mapping were performed on an FEI Titan Themis operated at 300 kV. TEM samples were prepared by dispersing the solid in ethanol (under sonication) and drop-casting the suspension onto lacey carbon-coated copper grids. Ru dispersion was estimated from TEM images assuming spherical particles, using the formula provided in the SI. Scanning electron microscopy (SEM) images and elemental maps were collected on a JEOL-7610F Plus equipped with an EDS detector. Powder X-ray diffraction (P-XRD) data were recorded on a Rigaku SmartLab diffractometer using monochromatic Cu Kα radiation ($\lambda = 0.154$ nm) at 40 kV and 30 mA in the 2θ range of 20° to 90°. X-ray photoelectron spectroscopy (XPS) was performed on a SPECS Surface Nano Analysis system (Germany) using Al Kα radiation (1486.61 eV); binding energies were charge-corrected to the C 1s signal (284.6 eV). Inductively coupled plasma optical emission spectroscopy (ICP-OES) was carried out on an Agilent 5800 instrument. For ICP-OES, the catalyst was digested in aqua regia in an autoclave at 180 °C for 4 h, then diluted with water prior to analysis. NMR spectra were recorded on Bruker Ascend 500 and Bruker Avance 400 spectrometers. Gas chromatography (GC) analyses were performed on a Shimadzu GC-2014 system equipped with a Shin Carbon-ST packed column and a thermal conductivity detector (TCD), using argon as the carrier gas. The TCD temperature was 200 °C, and the oven program was 90 °C (hold time 1 min), then 90–200 °C at 10 °C min^{-1}.

2.4. Catalytic test

Catalytic reactions were carried out in a 25 mL round-bottom flask equipped with a condenser and a water-displacement setup. Typically, the catalyst was dispersed in EG with the

required amounts of water and base. The reaction mixture was stirred at 600 rpm in an oil bath (100–140 °C) under an argon atmosphere. The evolved H_2 volume was measured using a calibrated water-displacement setup (4.0 ± 0.1 mL cm^{-1}), and gas composition was analyzed by GC–TCD. After completion, the catalyst was separated by centrifugation. Liquid products (formate and glycolate) were quantified by ^{1}H NMR using sodium acetate as an internal standard. Turnover frequencies (TOFs) were calculated based on total Ru content using the formula provided in the SI. Reported values represent the average of at least two independent experiments.

2.5. Recyclability experiment

Recycling tests were performed by reusing the recovered Ru/$La(OH)_3$ catalyst under identical conditions (EG (5 mmol), water (2 equiv.), NaOH (2.1 equiv.), 130 °C, Ar atmosphere). After each cycle, the catalyst was separated by centrifugation, washed with distilled water, dried under vacuum, and reused with fresh reactants.

2.6. Bulk experiment

Bulk-scale reactions were performed using EG (50 mmol) in a 50 mL round-bottom flask with water (2 equiv.) and NaOH (2.1 equiv.) in the presence of Ru/$La(OH)_3$ (100 mg) at 130 °C, following the standard procedure.

3. Results and discussion

3.1. Catalyst synthesis and characterization

Supported metal catalysts often provide improved metal dispersion, activity, stability, and reusability relative to unsupported counterparts.[41] Among common supports, metal hydroxides and oxides are particularly attractive due to their high surface area and thermal stability.[42,43] We synthesized a series of Ru catalysts by immobilizing Ru nanoparticles on $La(OH)_3$, γ-Al_2O_3, ZrO_2, CeO_2, and TiO_2 *via* wet impregnation followed by chemical reduction using $NaBH_4$. For Ru/$La(OH)_3$, the P-XRD pattern shows only reflections of $La(OH)_3$ (JCPDS 00-006-0585), with no detectable metallic Ru peaks, consistent with highly dispersed, small Ru nanoparticles (Fig. 1a). Similar patterns were observed for the other supported catalysts (Fig. S1). SEM-EDX and elemental mapping indicate uniform Ru dispersion across all samples (Fig. S2–S6), and ICP-OES confirms Ru loadings of 9–10 wt% (Table S2). TEM images of Ru/$La(OH)_3$ reveal Ru nanoparticles with an average size of *ca.* 1.5 nm dispersed on the $La(OH)_3$ support (Fig. 1b, c, e and Fig. S7). HAADF-STEM further distinguishes Ru nanoparticles (bright contrast) on the $La(OH)_3$ support (Fig. 1d). Consistent with EDS, wide-scan XPS confirms the presence of Ru, La, and O. Deconvolution of the Ru 3p spectrum shows peaks at 462.9 eV (Ru $3p_{3/2}$) and 485.2 eV (Ru $3p_{1/2}$), consistent with metallic Ru(0); a slight positive shift indicates electron-deficient Ru due to interactions with $La(OH)_3$ (Fig. 1f).[44] The Ru 3d spectrum shows peaks at 280.9 eV ($3d_{5/2}$) and 285.1 eV ($3d_{3/2}$), with the latter overlapping C 1s at 284.6 eV (Fig. S8). The La 3d spectrum exhibits doublets at 834.6 eV and 851.3 eV, assigned to La(III) $3d_{5/2}$ and $3d_{3/2}$, along with shake-up satellites at 837.9 eV and 854.6 eV (Fig. 1g). The O 1s spectrum shows peaks at 531.4 eV and 532.5 eV, assigned to La–O and surface-adsorbed water/hydroxyl groups, respectively (Fig. S9).

3.2. Catalytic dehydrogenation of ethylene glycol

The catalytic performance of the synthesized Ru/support catalysts (supports: $La(OH)_3$, CeO_2, γ-Al_2O_3, ZrO_2 and TiO_2) was evaluated for EG dehydrogenation to H_2 and formate in the presence of NaOH at 110 °C (Fig. 2a). Among the screened catalysts, Ru/$La(OH)_3$ showed the best performance, affording >99% EG conversion with selective formation of H_2 (176 mmol(H_2) g(Ru)$^{-1}$ h^{-1}) and 76% yield of sodium formate (SF) within 7 h (Table 1, entry 1). GC–TCD analysis confirmed that the evolved gas was pure H_2, with no detectable CO, CO_2, CH_4, or other impurities (Fig. 2c and Fig. S10). In contrast, Ru/CeO_2, Ru/γ-Al_2O_3, Ru/ZrO_2, and Ru/TiO_2 showed lower EG conversion, lower SF yields (28–40%), and longer reaction times (10 h) (Table 1, entries 2–5). On this basis, subsequent optimization studies were performed using Ru/$La(OH)_3$.

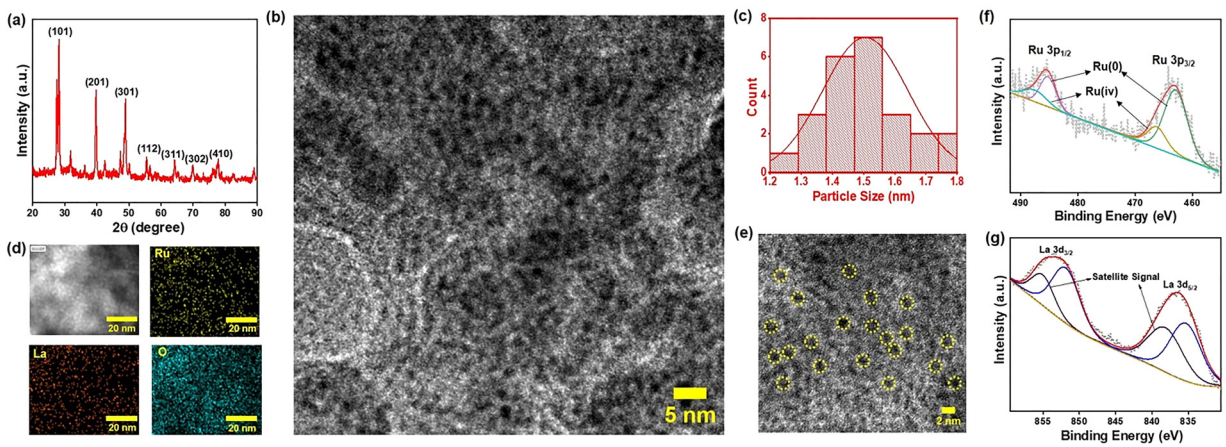

Fig. 1 (a) P-XRD, (b) TEM, (c) particle size distribution, (d) HAADF-STEM image and the corresponding elemental mappings, (e) TEM (Ru nanoparticles are highlighted by yellow circles), and XPS spectra of the (f) Ru 3p region and (g) La 3d region for the Ru/$La(OH)_3$ catalyst.

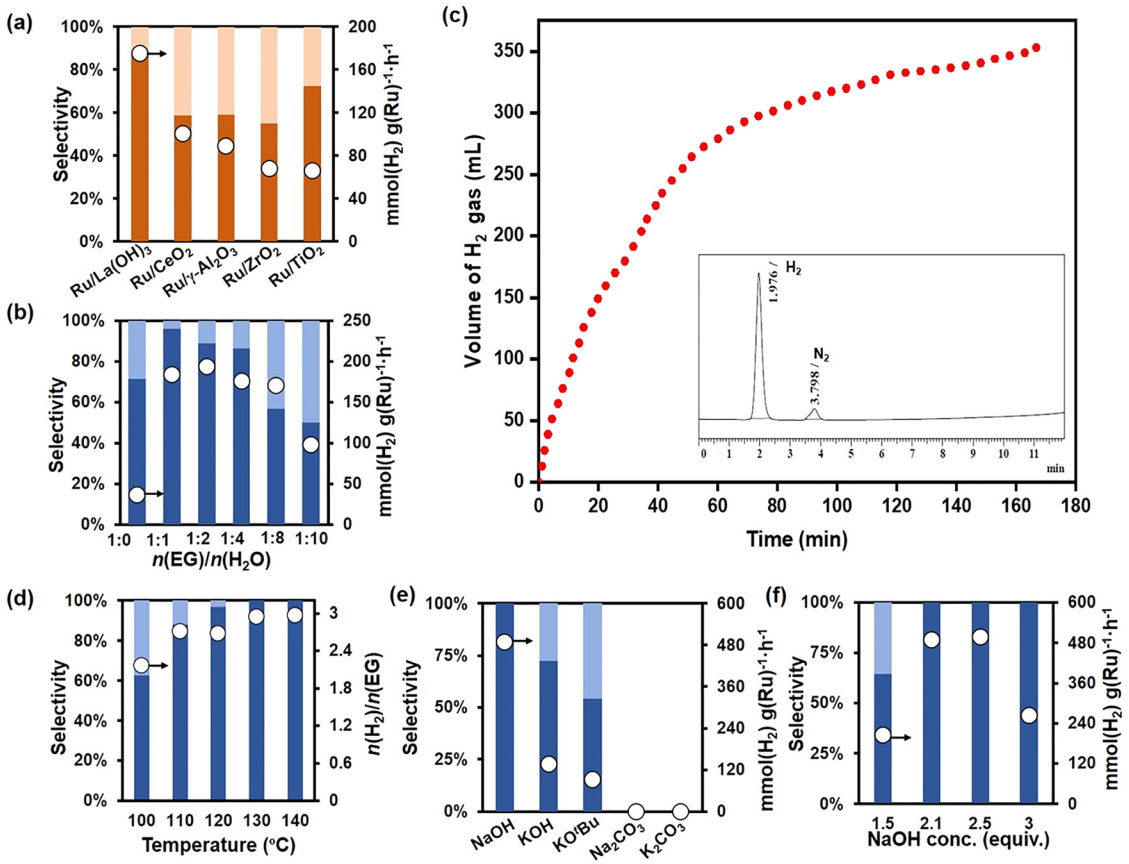

Fig. 2 (a) Screening of Ru/support catalysts for H_2 production from EG, and (b) effect of EG/H_2O ratio at 110 °C. (c) Time-course profile (GC–TCD data in the inset) for EG to H_2 at 130 °C. Effects of (d) reaction temperature (100–140 °C), (e) base identity, and (f) base concentration (1.5–3.0 equiv.). [Standard reaction conditions: Ru/La(OH)$_3$ (100 mg, 9 wt% Ru), EG (5 mmol), NaOH (2.1 equiv.), water (2 equiv.), 130 °C, and 600 rpm. Dark and light bars correspond to SF and SG, respectively].

Table 1 Optimization of the reaction conditions for hydrogen from ethylene glycol over the Ru/support catalysts[a]

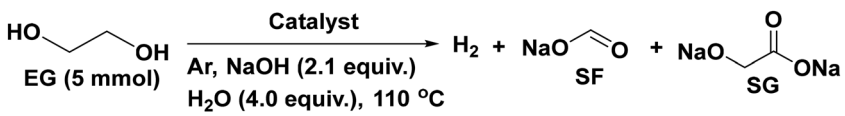

Entry	Catalyst	H_2[b] (mL)	t (h)	$n(H_2)/n(EG)$	Conv. (%)	Yield[c] of SF/SG (%)	Initial TOF[d] (h^{-1})	Productivity (mmol(H_2) $g(Ru)^{-1}$ h^{-1})
1	Ru/La(OH)$_3$	302	7	2.46	>99	76/11	61	176
2	Ru/CeO_2	246	10	2.00	94	39/27	24	100
3	Ru/γ-Al_2O_3	218	10	1.78	91	40/28	18	89
4	Ru/ZrO_2	166	10	1.36	81	28/22	11	68
5	Ru/TiO_2	162	10	1.32	68	39/15	8	66

[a] Reaction conditions: Ru/support (100 mg), EG (5 mmol), water (4 equiv.), NaOH (2.1 equiv.), 110 °C and 600 rpm. [b] Gas volume was measured using the water-displacement method. [c] Yield was determined by ^{1}H NMR using sodium acetate as an internal standard. [d] Turnover frequency (TOF) was calculated from the volume of H_2 released during the initial 1 h; TOF = TON/t. SF, sodium formate; SG, sodium glycolate; EG, ethylene glycol.

Using neat EG, only 55% conversion was obtained, with 102 mL of H_2 evolved (27.8% H_2 yield; $n(H_2)/n(EG) \approx 0.83$) over 11.5 h (Table S3, entry 1). Adding water markedly increased the conversion, likely by improving NaOH solubility and mass transfer. With 1 equiv. of water, H_2 evolution increased to 292 mL (79.8% H_2 yield) within 6.5 h (Table S3, entry 2). Increasing the water content to an EG/H_2O molar ratio of 1 : 2 gave 332 mL of gas (90.4% H_2 yield) in 10 h, with complete EG conversion and a high SF yield of ~82% (Table S3, entry 3). However, further dilution (EG/H_2O from 1 : 4 to 1 : 10) decreased EG conversion, presumably because lower effective EG concentration at the active sites reduces adsorption and

slows H_2 generation (Fig. 2c). These results underscore the importance of optimizing the EG/H_2O ratio to maximize selective conversion to H_2 and formate over Ru/La(OH)$_3$.

Increasing the reaction temperature from 100 to 140 °C accelerated H_2 evolution (E_a = 46 kJ mol^{-1}) and improved SF selectivity (Table S4 and Fig. S11 and S12). Optimal performance was obtained at 130 °C, where complete EG conversion was achieved with a quantitative H_2 yield and 94% SF yield within 3 h (Fig. 2d and Table S4, entry 4), highlighting the strong temperature dependence of both activity and selectivity. Replacing NaOH with other bases (KOH, KO^{t}Bu, Na_2CO_3, or K_2CO_3) lowered the EG conversion, underscoring the key role of base identity (Fig. 2e and Table S5). Varying the NaOH loading from 1.5 to 3.0 equiv. increased H_2 production and conversion, with the best results at 2.1 equiv. NaOH. Under these conditions, 360 mL of H_2 (98% yield) was produced at a rate of 490 mmol(H_2) g(Ru)$^{-1}$ h^{-1} at 130 °C (Fig. 2f and Table S6, entry 2). Complete conversion was also achieved with a lower Ru loading (5 wt%) in Ru/La(OH)$_3$, although with a lower production rate (468 mmol(H_2) g(Ru)$^{-1}$ h^{-1} in 6 h) compared to 9 wt% Ru (490 mmol(H_2) g(Ru)$^{-1}$ h^{-1} in 3 h) at 130 °C (Table S7, entry 2; Fig. S13).

Furthermore, *in situ* FT-IR experiments were performed to probe the role of Ru/La(OH)$_3$ in EG activation by monitoring adsorption of EG and key intermediates on the catalyst surface (Fig. 3). As shown in Fig. 3b, adsorption of EG, glyoxal (GLOX), and glycolic acid (GA) on Ru/La(OH)$_3$ at room temperature gave characteristic bands at 1068, 1555, and 1658 cm^{-1}, respectively, which are assigned to the C–O and C═O stretching vibrations of the corresponding adsorbed oxygenated species.[45] In addition, GA exhibited a distinct band at 1376 cm^{-1}, assigned to the symmetric stretching vibration of the COO$^-$ group.[46] Similarly, formic acid adsorbed on Ru/La(OH)$_3$ at room temperature showed characteristic bands at 1577 cm^{-1} [ν_{as}(COO$^-$)], 1350 cm^{-1} [ν_s(COO$^-$)], and 2870 cm^{-1} [ν_s(C–H)]. Upon heating the EG-adsorbed Ru/La(OH)$_3$ catalyst to 130 °C, the emergence of bands at 1577 and 1350 cm^{-1}, assigned to the asymmetric and symmetric COO$^-$ stretching vibrations of formate, along with the 2870 cm^{-1} C–H stretching vibration, inferred the formation of surface formate species during EG dehydrogenation.[47] The time-dependent *in situ* FT-IR spectra (Fig. 3c) showed that the characteristic bands for EG adsorption at 1068 cm^{-1} and an increase in the band for ate at 2870 cm^{-1} with progress of reaction time to 130 °C. Furthermore, temperature-dependent and time-resolved ^{1}H NMR also revealed the involvement of a glycolate intermediate during the dehydrogenative conversion of EG to formate (Fig. S14). As shown in Fig. 3d, increasing the reaction temperature (100–140 °C) led to a progressive increase in the intensity of SF peaks, while the intensity of the peaks for the SG intermediate, which appeared strong at 100 °C, gradually decreased and disappeared completely at 130 °C. Similarly, the time-resolved ^{1}H NMR spectra at 130 °C (Fig. 3e) showed a distinct increase in the intensity of the peaks of formate, while peaks corresponding to glycolate decrease with the increase in the reaction duration. Collectively, these spectroscopic results demonstrated that during EG dehydrogenation to formate, glycolate was possibly involved as a key intermediate species.

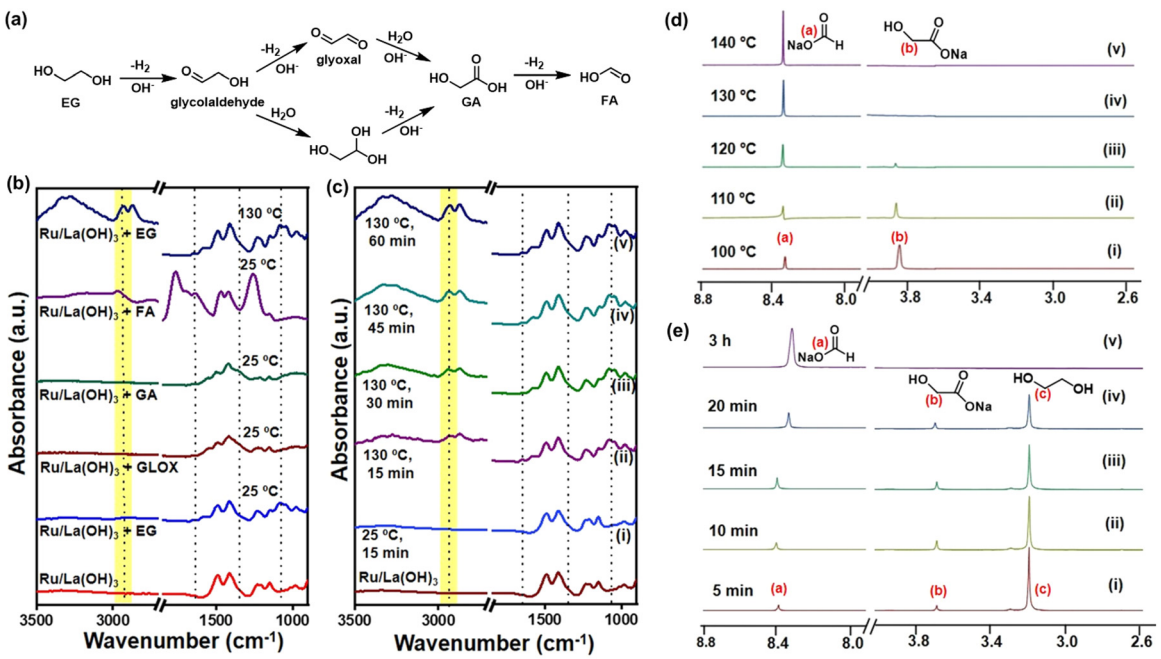

Fig. 3 (a) Plausible reaction pathway for hydrogen production from EG over the Ru/La(OH)$_3$ catalyst, FT-IR spectra of (b) Ru/La(OH)$_3$ after adsorption of EG, GLOX, GA, and FA, (c) time-dependent FT-IR spectra of Ru/La(OH)$_3$ with adsorption of EG, (d) temperature-dependent and (e) time-dependent ^{1}H NMR spectra of EG dehydrogenation over Ru/La(OH)$_3$. [Reaction conditions: Ru/La(OH)$_3$ (100 mg, 9 wt% Ru), ethylene glycol (5 mmol), NaOH (10.5 mmol), water (10 mmol), 130 °C, and 600 rpm]. EG (ethylene glycol), GLOX (glyoxal), GA (glycolic acid), and FA (formic acid).

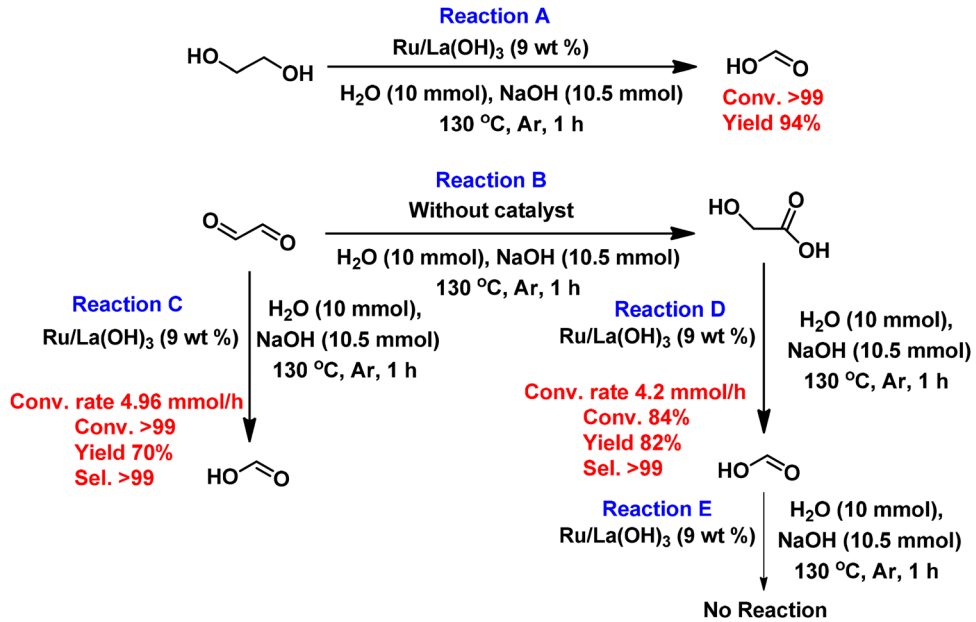

Scheme 2 Control experiments to elucidate the reaction pathway for EG to H_2 gas and formate transformation.

To further elucidate the reaction pathway, a series of control experiments was conducted (Scheme 2), with reference to the optimized standard conditions (Scheme 2, Reaction A, Fig. S15), where complete conversion of EG was observed with 94% yield of SF over Ru/La(OH)$_3$ at 130 °C. A control experiment with glyoxal showed the quantitative yield of SG in the presence of NaOH under catalyst-free conditions, suggesting that glyoxal to glycolate is a base-promoted rearrangement pathway (Scheme 2, Reaction B, Fig. S16). In contrast, glyoxal underwent catalytic dehydrogenation over Ru/La(OH)$_3$ at 130 °C to afford SF (sel. >99% and conversion rate 4.96 mmol h^{-1}) with the evolution of H_2 gas (3.54 mmol) (Scheme 2, Reaction C, Fig. S17). Similarly, GA converted to SF with the release of H_2 gas over the Ru/La(OH)$_3$ catalyst in the presence of 2.1 equiv. of NaOH, with a conversion rate of 4.2 mmol h^{-1} (Scheme 2, Reaction D, Fig. S18), while Ru/CeO_2, Ru/ZrO_2 and Ru/TiO_2 showed poor conversion rates of, respectively, 2.2, 0.7 and 0.3 mmol h^{-1} (Table S8), suggesting the crucial role of the basic support in achieving enhanced dehydrogenation of EG to SF (Fig. S19). However, further transformation of FA or SF to H_2 was not observed over the Ru/La(OH)$_3$ catalyst (Scheme 2, Reaction E, Fig. S20).

Notably, earlier reports showed that basic supports promoted polyol reforming and dehydrogenation by facilitating alcohol activation, intermediate conversion, and improved hydrogen selectivity. For instance, Guo *et al.* reported that glycerol aqueous-phase reforming over Pt/support catalysts followed the activity order of Pt/MgO > Pt/Al_2O_3 > Pt/CeO_2 > Pt/TiO_2 > Pt/SiO_2, demonstrating the beneficial role of support basicity.[48] Similarly, Boga *et al.* showed that basic Mg(Al)O supported enhanced H_2 selectivity in glycerol reforming.[49] In line with these reports, CO_2-TPD profiles of Ru/La(OH)$_3$, Ru/CeO_2, Ru/γ-Al_2O_3, Ru/ZrO_2, and Ru/TiO_2 revealed distinct differences in their basic site strength (Fig. S21), where Ru/La(OH)$_3$ exhibited moderate-to-strong basic sites,[41] Ru/CeO_2 and Ru/γ-Al_2O_3 showed weak-to-moderate basic sites,[50–53] while Ru/ZrO_2 and Ru/TiO_2 possessed only weak basic sites.[41,48] The observed trend in basic sites of the screened catalysts aligned well with their catalytic activity for EG dehydrogenation: Ru/La(OH)$_3$ > Ru/CeO_2 > Ru/γ-Al_2O_3 > Ru/ZrO_2 > Ru/TiO_2. Accordingly, these findings highlight the crucial role of the support material in cooperation with the Ru site in achieving high catalytic activity for EG dehydrogenation, where Ru/La(OH)$_3$ outperformed others to achieve complete conversion of EG. Therefore, based on these findings, the pathway for EG dehydrogenation is proposed to have the following steps (Fig. 3a), where EG undergoes initial dehydrogenation to glycolaldehyde, followed by base-assisted dehydrogenation to glyoxal. The resulting glyoxal is then converted to GA either through a base-promoted rearrangement or *via* hydration to a geminal diol followed by dehydrogenation. Finally, GA undergoes catalytic dehydrogenation to produce FA with the release of H_2.

Notably, EG is a key component of polyethylene terephthalate (PET) and can be released from PET waste *via* hydrolysis, alcoholysis, or related depolymerization processes. To broaden the scope of the developed system, we therefore evaluated a simultaneous depolymerization cum dehydrogenation of PET waste under analogous reaction conditions. At 130 °C, complete PET conversion was achieved within 1 h, accompanied by an H_2 yield of 15.3 mmol g(PET)$^{-1}$ (for the transformation of PET to H_2 and formate: theoretical maximum yield of H_2 is 15.6 mmol g(PET)$^{-1}$) over Ru/La(OH)$_3$, corresponding to a production rate of 294 mmol (H_2) g(Ru)$^{-1}$ h^{-1} (Fig. S22 and S23). This performance is over two-fold higher than that of unsupported Ru nanoparticles (115 mmol(H_2) g(Ru)$^{-1}$ h^{-1}), clearly

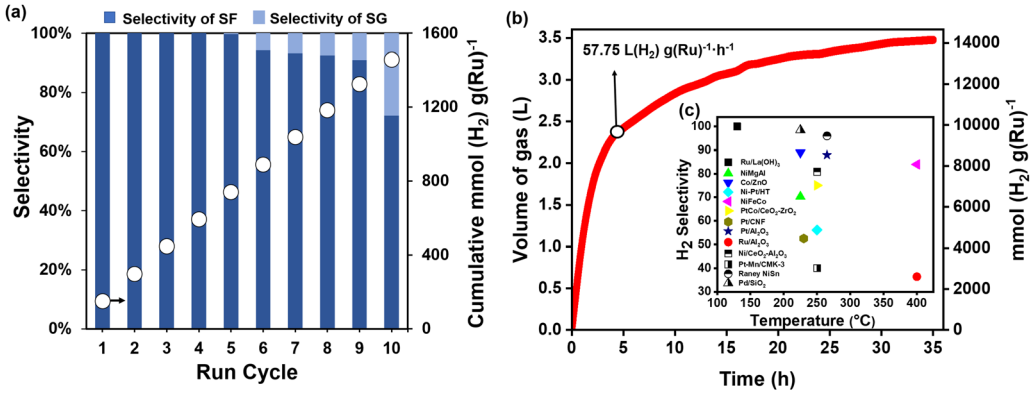

Fig. 4 (a) Recyclability test for H_2 production from EG over Ru/La(OH)$_3$. Reaction conditions: Ru/La(OH)$_3$ (100 mg, 9 wt% Ru), EG (5 mmol), NaOH (10.5 mmol), water (10 mmol), 130 °C, 600 rpm. (b) Time-course profile for H_2 production from bulk-scale EG over Ru/La(OH)$_3$. Reaction conditions: Ru/La(OH)$_3$ (100 mg, 9 wt% Ru), EG (50 mmol), NaOH (105 mmol), water (100 mmol), 130 °C, 600 rpm. (c) Comparison of this work with literature reports on EG dehydrogenation over heterogeneous catalysts.

demonstrating the superior catalytic performance of the Ru/La(OH)$_3$ catalyst for complete dehydrogenation of PET.[54]

3.3. Catalyst stability and recyclability

A mercury-poisoning test was performed to examine the heterogeneous nature of Ru/La(OH)$_3$. Upon addition of excess elemental Hg, the reaction quenched significantly, consistent with poisoning of surface Ru sites and hence supporting the heterogeneous nature of the Ru/La(OH)$_3$ catalyst (Fig. S24). The durability of Ru/La(OH)$_3$ was further demonstrated by the recovery and reuse of the catalyst over ten consecutive cycles for EG dehydrogenation at 130 °C, with no significant loss of activity (Fig. S25). The catalyst maintained excellent H_2 selectivity, reaching a cumulative TON of 14 395 mol(H_2) mol(Ru)$^{-1}$ (350 L(H_2) g(Ru)$^{-1}$) with an average production rate of 7.6 L(H_2) g(Ru)$^{-1}$ h^{-1} and $n(H_2)/n(EG) \approx 2.86$ (Fig. 4a). This performance exceeds that of previously reported necked Ru nanoparticle catalysts (~2.4 L(H_2) g(Ru)$^{-1}$ h^{-1}),[40] highlighting the beneficial role of the La(OH)$_3$ support under the optimized conditions.

The Ru/La(OH)$_3$ catalyst also showed good scalability, producing ~3.5 L of H_2 (14 300 mmol(H_2) g(Ru)$^{-1}$) from 50 mmol EG in 35 h at 130 °C, corresponding to an average rate of ~10 L(H_2) g(Ru)$^{-1}$ h^{-1}. Notably, ~2.3 L of H_2 (~66% of the total) was generated within the first 4 h, giving a peak rate of ~58 L(H_2) g(Ru)$^{-1}$ h^{-1} (Fig. 4b). Under identical conditions, the supported Ru/La(OH)$_3$ catalyst delivered a substantially higher hydrogen yield ($n(H_2)/n(EG) \approx 2.86$ in 35 h) than unsupported Ru (~2.5 L(H_2) g(Ru)$^{-1}$ h^{-1}; $n(H_2)/n(EG) \approx 1.1$ in 52 h).[40] Post-reaction XRD, TEM, and HAADF-STEM analyses, along with elemental mapping of Ru/La(OH)$_3$, showed no obvious structural changes (Fig. S25). Previously reported catalysts for EG dehydrogenation typically operate under relatively harsh conditions (225–400 °C), often require longer reaction times and/or elevated pressures, and can generate carbon-containing gaseous by-products such as CO, CO_2, CH_4, or light alkanes, which lowers hydrogen selectivity (Fig. 4c). In contrast, Ru/La(OH)$_3$ delivers excellent performance at a much milder temperature of 130 °C, achieving complete EG conversion within 3 h with 94% formate yield and >99% H_2 selectivity, while producing no detectable CO, CO_2, or CH_4.

Overall, these findings demonstrated that immobilizing Ru nanoparticles on La(OH)$_3$ markedly enhanced catalytic EG dehydrogenation over Ru/La(OH)$_3$ compared to unsupported Ru nanoparticles.[40] The Ru/La(OH)$_3$ catalyst exhibited a two-fold increase in activity, achieving an initial TOF of 61 h^{-1} with 87% SF selectivity at 110 °C, compared to a TOF of 32 h^{-1} and 68% SF selectivity for unsupported Ru nanoparticles. Even at 130 °C, the Ru/La(OH)$_3$ catalyst maintained superior activity of 147 h^{-1}, compared to 67 h^{-1} for unsupported Ru nanoparticles.[40] A distinct advantage with the Ru/La(OH)$_3$ catalyst was observed during bulk scale EG dehydrogenation (50 mmol), delivering an exceptional productivity of 10 L(H_2) g(Ru)$^{-1}$ h^{-1} (TON of 14 300 mmol(H_2) g(Ru)$^{-1}$ with $n(H_2)/n(EG) \approx 2.86$), surpassing the activity of unsupported Ru nanoparticles (2.4 L(H_2) g(Ru)$^{-1}$ h^{-1}) by over four-fold.[40] These findings demonstrate that the strategy of immobilizing Ru over La(OH)$_3$ goes beyond a modest improvement in catalytic activity, to achieve enhanced catalyst recyclability, high formate selectivity and H_2 productivity, attributed to the cooperative interplay between Ru sites and the basic La(OH)$_3$ support.

4. Conclusion

In summary, a Ru/La(OH)$_3$ catalyst was explored for low-temperature, selective reforming of ethylene glycol (EG) to CO_2-free hydrogen and formate in aqueous alkaline media. The catalyst enables complete EG conversion at 130 °C, delivering quantitative H_2 yield (2.94 mol H_2 per mol EG) together with a high formate yield (94%). The catalyst remains active over ten consecutive cycles and achieves a cumulative TON of 14 395 mol(H_2) mol(Ru)$^{-1}$ (142.5 mol(H_2) g(Ru)$^{-1}$). On the bulk scale (50 mmol EG), ~3.5 L of H_2 was produced (1250 L(H_2) L(EG)$^{-1}$) at 130 °C. The same catalyst also enables a one-pot PET waste depolymerization that generates a high yield of purified hydrogen, alongside terephthalate and formate. Control experiments and *in situ* FTIR measurements

support a key role for the catalyst in promoting favorable adsorption of EG and reactive intermediates involved in the process of EG dehydrogenation. Overall, this work demonstrates CO_2-free H_2 production with the co-production of high-value formate from EG-derived feedstocks.

Conflicts of interest

There are no conflicts to declare.

Data availability

The data supporting this article have been included as part of the supplementary information (SI). The supplementary information contains detailed experimental procedures, catalyst characterization data, reaction optimization and control experiments, spectroscopic analyses, catalytic performance data, recyclability studies, and additional supporting figures and tables. See DOI: https://doi.org/10.1039/d6ma01168c.

Acknowledgements

This work was supported by the PAIR Network of SAKSHAM, funded by ANRF (Anusandhan National Research Foundation), India (ANRF/PAIR/2025/000018/PAIR), administered and mentored by IIT Indore. The authors acknowledge the DST-FIST 500 MHz NMR facility, the Department of Chemistry, and the Sophisticated Instrumentation Centre (SIC), IIT Indore, for instrumentation support. The XPS facility at CIF UGC-DAE and the TEM facility at IIT Gandhinagar are also gratefully acknowledged. The authors thank the Catalysis Group, IIT Indore, for valuable discussions and suggestions. S. M. acknowledges DST-INSPIRE for fellowship support.

References

1 M. Balat, *Int. J. Hydrogen Energy*, 2008, **33**, 4013–4029.
2 A. M. Sadeq, R. Z. Homod, A. K. Hussain, H. Togun, A. Mahmoodi, H. F. Isleem, A. R. Patil and A. H. Moghaddam, *Sci. Total Environ.*, 2024, **939**, 173622.
3 S. Anil, S. Indraja, R. Singh, S. Appari and B. Roy, *Int. J. Hydrogen Energy*, 2022, **47**, 8177–8213.
4 M. M. H. Bhuiyan and Z. Siddique, *Int. J. Hydrogen Energy*, 2025, **102**, 1026–1040.
5 B. Loges, A. Boddien, H. Junge and M. Beller, *Angew. Chem., Int. Ed.*, 2008, **47**, 3962–3965.
6 A. Fasolini, G. Martelli, A. Piazzi, M. Curcio, J. De Maron, F. Basile and R. Mazzoni, *ChemCatChem*, 2024, **16**, e202400393.
7 D. Mellmann, P. Sponholz, H. Junge and M. Beller, *Chem. Soc. Rev.*, 2016, **45**, 3954–3988.
8 A. Boddien, D. Mellmann, F. Gärtner, R. Jackstell, H. Junge, P. J. Dyson, G. Laurenczy, R. Ludwig and M. Beller, *Science*, 2011, **333**, 1733–1736.
9 S. Patra, H. Deka and S. K. Singh, *Inorg. Chem.*, 2021, **60**, 14275–14285.
10 I. Yuranov, N. Autissier, K. Sordakis, A. F. Dalebrook, M. Grasemann, V. Orava, P. Cendula, L. Gubler and G. Laurenczy, *ACS Sustainable Chem. Eng.*, 2018, **6**, 6635–6643.
11 S. Patra and S. K. Singh, *Inorg. Chem.*, 2020, **59**, 4234–4243.
12 L. E. Heim, N. E. Schlörer, J. H. Choi and M. H. G. Prechtl, *Nat. Commun.*, 2014, **5**, 1–8.
13 M. Trincado, V. Sinha, R. E. Rodríguez-Lugo, B. Pribanić, B. de Bruin and H. Grützmacher, *Nat. Commun.*, 2017, **8**, 1–11.
14 T. A. Kharde and S. K. Singh, *Energy Fuels*, 2024, **38**, 15848–15854.
15 M. Nielsen, E. Alberico, W. Baumann, H. J. Drexler, H. Junge, S. Gladiali and M. Beller, *Nature*, 2013, **495**, 85–89.
16 L. Lin, W. Zhou, R. Gao, S. Yao, X. Zhang, W. Xu, S. Zheng, Z. Jiang, Q. Yu, Y.-W. Li, C. Shi, X.-D. Wen and D. Ma, *Nature*, 2017, **544**, 80–83.
17 M. K. Awasthi, R. K. Rai, S. Behrens and S. K. Singh, *Catal. Sci. Technol.*, 2021, **11**, 136–142.
18 T. V. Haasterecht, T. W. van Deelen, K. P. de Jong and J. H. Bitter, *Catal. Sci. Technol.*, 2014, **4**, 2353–2366.
19 L. Xie, Z. Huang, Y. Zhan, J. Huang, C. Wang, R. Shu, J. Wang, L. Lei, J. Liu, Z. Tian and Y. Chen, *Catalysts*, 2025, **15**, 258.
20 A. Fasolini, R. Cucciniello, E. Paone, F. Mauriello and T. Tabanelli, *Catalysts*, 2019, **9**, 917.
21 L. Leroy, A. Koul, F. B. S. Nkou, J. P. Fandre, A. Hareendran, G. W. Busser, H. Tüysüz, S. Kenmoe, W. Schuhmann and M. Muhler, *Angew. Chem., Int. Ed.*, 2026, **65**, e19188.
22 Y. Q. Zou, N. V. Wolff, M. Rauch, M. Feller, Q. Q. Zhou, A. Anaby, Y. Diskin-Posner, L. J. W. Shimon, L. Avram, Y. Ben-David and D. Milstein, *Chem. – Eur. J.*, 2021, **27**, 4715–4722.
23 Y. Q. Zou, N. V. Wolff, A. Anaby, Y. Xie and D. Milstein, *Nat. Catal.*, 2019, **2**, 415–422.
24 S. T. Sahoo, A. Mohanty, R. Sharma and P. Daw, *Dalton Trans.*, 2023, **52**, 15343.
25 Y. Zhan, W. Hou, G. Li, Y. Shen, Y. Zhang and Y. Tang, *ACS Sustainable Chem. Eng.*, 2019, **7**, 17559–17564.
26 S. Waiba, M. Maiti and B. Maji, *ACS Catal.*, 2022, **12**, 3995–4001.
27 R. Sundari and P. D. Vaidya, *Chem. Eng. Commun.*, 2015, **202**, 1446–1454.
28 A. D. Kiadehi and M. Taghizadeh, *Int. J. Hydrogen Energy*, 2018, **43**, 4826–4838.
29 X. L. Zhao, Y. A. Lü, W. P. Liao, M. S. Jin and Z. H. Suo, *J. Fuel Chem. Technol.*, 2015, **43**, 581–588.
30 R. D. Cortright, R. R. Davda and J. A. Dumesic, *Nature*, 2002, **418**, 964–967.
31 Y. Wang, M. Chen, X. Li, Z. Yang, T. Liang, Z. Zhou and Y. Cao, *Int. J. Hydrogen Energy*, 2018, **43**, 20438–20450.
32 A. D. Shejale and G. D. Yadav, *Int. J. Hydrogen Energy*, 2021, **46**, 4808–4826.
33 D. Mei, V. L. Dagle, R. Xing, K. O. Albrecht and R. A. Dagle, *ACS Catal.*, 2016, **6**, 315–325.
34 A. Larimi and F. Khorasheh, *Renewable Energy*, 2018, **128**, 188–199.

35 X. Chu, J. Liu, B. Sun, R. Dai, Y. Pei, M. Qiao and K. Fan, *J. Mol. Catal. A: Chem.*, 2011, **335**, 129–135.
36 S. Jeon, Y. M. Park, K. Saravanan, G. Y. Han, B. W. Kim, J. B. Lee and J. W. Bae, *Int. J. Hydrogen Energy*, 2017, **42**, 9892–9902.
37 H. D. Kim, H. J. Park, T. W. Kim, K. E. Jeong, H. J. Chae, S. Y. Jeong, C. H. Lee and C. U. Kim, *Int. J. Hydrogen Energy*, 2012, **37**, 8310–8317.
38 R. R. Davda, J. W. Shabaker, G. W. Huber, R. D. Cortright and J. A. Dumesic, *Appl. Catal., B*, 2003, **43**, 13–26.
39 G. W. Huber, J. W. Shabaker and J. A. Dumesic, *Science*, 2003, **300**, 2075–2077.
40 A. Kumar, B. Priya and S. K. Singh, *ACS Sustainable Chem. Eng.*, 2023, **11**, 3999–4008.
41 A. Kumar, B. Priya, R. K. Rai, P. Garg, U. Deshpande and S. K. Singh, *Energy Adv.*, 2025, **4**, 106.
42 Z. Alhalili, *Molecules*, 2023, **28**, 3086.
43 S. Abate, C. Mebrahtu, E. Giglio, F. Deorsola, S. Bensaid, S. Perathoner, R. Pirone and G. Centi, *Ind. Eng. Chem. Res.*, 2016, **55**, 4451–4460.
44 B. Priya, A. Kumar and S. K. Singh, *Sustainable Energy Fuels*, 2024, **8**, 4376.
45 J. Gomes, A. Garcia, L. Gasparotto, N. D. Souza, E. Ferreira, C. Pires and G. T. Filho, *Electrochim. Acta*, 2014, **144**, 361.
46 L. Wang, H. Meng, P. K. Shen, C. Bianchini, F. Vizzab and Z. Weic, *Phys. Chem. Chem. Phys.*, 2011, **13**, 2667–2673.
47 S. Bhattacharjee, U. Pulikkeel, V. Amoli, M. Sk, R. Thapa, B. Chowdhury, T. E. Müller, P. K. Chinthala and A. Bhaumik, *Adv. Funct. Mater.*, 2025, **35**, 2502434.
48 Y. Guo, M. U. Azmat, X. Liu, Y. Wang and G. Lu, *Appl. Energy*, 2012, **92**, 218–223.
49 D. A. Boga, R. Oord, A. M. Beale, Y. M. Chung, P. C. A. Bruijnincx and B. M. Weckhuysen, *ChemCatChem*, 2013, **5**, 529–537.
50 Y. He, D. Mao, Q. Guo and J. Yu, *Fuel Process. Technol.*, 2024, **259**, 108101.
51 T. Sakpal and L. Lefferts, *J. Catal.*, 2018, **367**, 171–180.
52 L. M. Brave, F. C. Meunier and J. Kopyscinski, *Appl. Catal., B*, 2025, **361**, 124591.
53 G. Ralengole, K. Jalama and P. Khangale, *Heliyon*, 2024, **10**, e31349.
54 A. Kumar, M. K. Awasthi, N. Sheet, T. A. Kharde and S. K. Singh, *ChemCatChem*, 2023, **15**, e202300574.

